

***Ab Initio* Simulation of Materials for Environmentally Friendly Technologies**

Jarek Dąbrowski, Fatima Akhtar, Max Franck, and Mindaugas Lukosius

IHP – Leibniz-Institut für innovative Mikroelektronik,
Im Technologiepark 25, 15236 Frankfurt (Oder), Germany
E-mail: dabrowski@ihp-microelectronics.com

An *ab initio* DFT study of nucleation and growth of graphene and hBN for high-performance environmentally friendly microelectronics and of N and O co-doping of activated carbon for metal-free catalysis is reported. As fringe benefit, a new Ge(110) surface structure was revealed.

1 Introduction

The need for environmentally friendly technologies in response to global climate change necessitates innovation in materials. Simulations support these innovations by providing insights into complex physical processes and guiding experimental efforts. When the approximations used are well-founded in physics, simulations reduce intuitive bias while fostering reliable physical intuition comparable to insights gained from experiments. *Ab initio* density functional theory (DFT) falls into this category, as it operates at the quantum-mechanical level of atomic interactions. Although computationally intensive (which limits its use), it is indispensable for modern technology development, especially in the design and optimisation of materials at the atomic scale. By integrating theoretical and experimental insights, DFT simulations contribute to breakthroughs in material design, paving the way for greener solutions. This includes microelectronics, where innovative ideas applied on the atomistic level can help mitigate environmental impacts associated with cost-driven performance improvements and miniaturisation, while also reducing energy consumption.

For instance, Cu ion contamination is a concern in water pollution caused by the semiconductor industry^{1,2}. The costs of removing Cu from wastewater are an important factor³. With the growing adoption of graphene (sheets of sp²-bonded C atoms), which is typically synthesised on Cu, this issue is expected to intensify, as copper released during etching and transfer⁴⁻⁶ increases filtration costs and environmental risks. Cu from graphene production may also contaminate devices and fabrication lines^{7,8}, compounding the financial and environmental pressures for innovative solutions. To address these challenges, the IHP is exploring the option of growing graphene on semiconductor substrates where feasible⁹⁻¹⁴.

This work continues our previous studies¹⁵⁻¹⁹ done at the IHP with the support of the John von Neumann Institute for Computing. We present selected results of our recent *ab initio* DFT calculations run on the JUWELS cluster. The discussion focuses on the nucleation and growth mechanisms of two-dimensional (2D) films for modern microelectronics: graphene⁹⁻¹³ (Sec. 2) and hexagonal boron nitride (hBN)²⁰⁻²⁴ (Sec. 3). In addition, the role of N and O co-doping in adsorption processes contributing to catalytic activity of activated carbon²⁵ (Sec. 4.1) is addressed and a concept of low-energy Ge(110) surface reconstruction reconciling two opposing models^{26,27} (Sec. 4.2) is introduced.

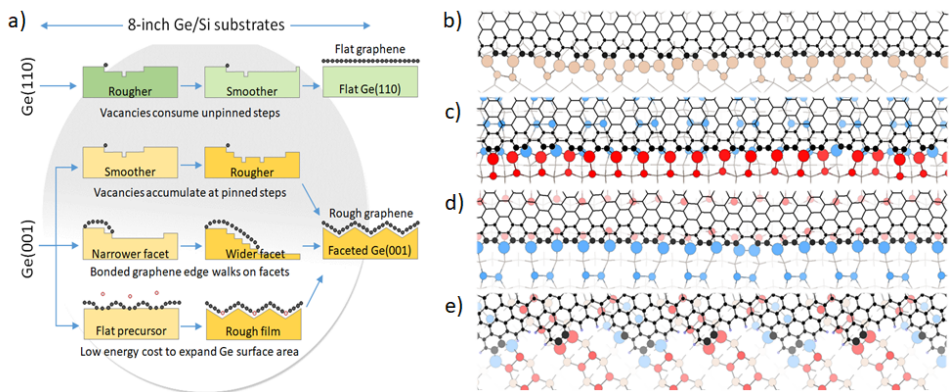


Figure 1. (a) The factors contributing to the response of Ge(110) and Ge(001) surfaces to graphene growth¹². (b-e) Graphene bonded to straight steps on: (b) Ge(110) and (c-d) on Ge(001), and (e) to a flat Ge(001) with some Ge dimer vacancy clusters attracted to the bonding front. The red and blue circles in the Ge(001) panels indicate the atoms of the two Ge dimerisation domains: the dimers in domain A are perpendicular to those in domain B. The elevation difference between the domains corresponds to a monatomic step height and equals to the depth of a dimer vacancy. The panel (e) illustrates the initial stage of roughening by (107) facet formation.

2 Graphene on Germanium Surfaces

Graphene is a sheet of sp^2 -bonded carbon atoms. Among other applications, it is considered to be the fundamental material to enable technological breakthrough in microelectronics through synergistic combination of multiple 2D films and silicon technology²⁸. The IHP evaluates its potential for usage in high-frequency transistors, in optical interconnects, and in sensors. The Materials Research department of IHP investigates the growth of graphene on Ge wafers and on Si wafers covered by Ge layers (Ge/Si), in the lab as well as under conditions relevant to mass production¹²⁻¹⁴. For this study, graphene layers were grown by chemical vapour deposition (CVD) on Ge from CH_4 and H_2 mixture at about $850^\circ C$. This is by roughly $150^\circ C$ less than when grown on Cu, which may reduce the energy consumption⁶, making this technology more friendly to the environment than the usual approach.

Ge(110) and Ge(001) surfaces respond differently to the same growth conditions: Ge(110) flattens and Ge(001) roughens. Fig. 1a collects the key factors causing this difference, as revealed by our work. It builds on the combination of extensive experimental work and the results of numerous DFT calculations for the total energies of atomic structures, for the energy barriers between the most important structures, the kinetic paths to their formation, and the experimental conditions. The analysis required knowledge on the surface energy differences, which are difficult to obtain from experiment (Sec. 4.2). Furthermore, the information gathered by us for these systems previously^{9,29,10} was accounted for. This includes the energetics and kinetics of CH_4 adsorption and decomposition and the hypotheses on the formation mechanism of the (107) facets on Ge(001). The following discussion illustrates some of the aspects involved.

A clean Ge surface is reactive against CH_4 , causing the impinging molecules to dissociate step by step down to single C and H atoms. When exposed to CH_4 , the surface

becomes initially covered by a mixture of CH_4 fragments and their polymers. The composition and concentration of this mixture depends on the substrate temperature, on the partial pressures of CH_4 and H_2 , and – locally – on the size of the graphene nucleus that by chance has been formed within about a micrometer from the site of interest, *i. e.*, within the distance covered by an average C atom before it eventually dissolves in the bulk.

The smallest of these nuclei contain few C atoms and are mobile. They combine into larger, already immobile flakes. Van der Waals forces orient them parallel to the surface. Such a flake prefers to be attached to a surface step (Fig. 1b-d) rather than to the flat surface (Fig. 1e) because the in latter case it must be bent along the edge, which costs energy.

Being immobile, however, the larger flakes appear at random sites, not necessarily at steps. Yet the bonded Ge(001)-graphene boundary attracts mobile native defects (Ge adatoms, ad-dimers, surface vacancies). This creates new surface steps along the flakes. Furthermore, the flakes on Ge(001) can minimise their lateral strain as well. They achieve this by a slight rotation with respect to Ge dimer rows (Fig. 1e), which happens to orient the bonded boundary along the line of crossing between the Ge(001) and Ge(107) planes. The surface energy of Ge(107) is relatively low, so a (107) facet can extend away from the boundary. We verified that the flake can expand itself onto the facet simply by enlarging its “fingers” visible in Fig. 1e and then filling the regions between them with graphene. Eventually, the Ge(001) surface develops a system of (107) nano-facets (Fig. 1a), so that more CH_4 can convert into low-strained graphene than it would be possible on a flat Ge(001).

This is in opposition to what happens on Ge(110). While the reconstruction of Ge(001) is simple (just dimerisation of the surface atoms), Ge(110) has an intricate structure with sizeable building blocks (Sec. 4.2), which hinders the formation of graphene-induced facets. The alternative, preferred scenario is then that instead of accumulating in front of the bonded flake to form a new terrace (which would lead to surface roughening) the Ge vacancies produced by GeH_4 desorption^a consume Ge(110) step edges, gradually removing the existing islands and making the surface smoother and smoother (Fig. 1a).

3 Hexagonal BN

Monolayer hBN is a 2D wide band-gap insulator with hexagonal lattice and atomic structure that resembles that of graphene (which is a 2D metal). Both materials have the form of a 2D honeycomb built of hexagonal atomic rings (C_6 in graphene, B_3N_3 in hBN). The lattice constant of hBN is by 1.7% larger than that of graphene.

Apart from optimising the graphene/Ge/Si growth recipe, we attempted the growth of heterostructures on Ge/Si and on Si, consisting of monolayer graphene and multilayer hBN films. Here we discuss the growth of the first hBN layer on Ge(001) and then the growth of subsequent hBN layers, that is, the growth of hBN on hBN.

The purpose of the calculations was to reveal the reactions of $\text{B}_x\text{N}_y\text{H}_z$ species with the substrate, the nucleation and expansion of seeds, and the kinetics of generation and annihilation of defects²⁰⁻²⁴. To address the posed questions one must treat a huge number of structures and structural transitions (our associated database contains by now more than 30k items), of size varying from isolated atoms and molecules, through isolated or periodic clusters of 100-200 atoms, up to periodic clusters consisting of more than a thousand atoms. The access to the JUWELS cluster was therefore crucial for this project.

^aHydrogen comes from CH_4 and from H_2

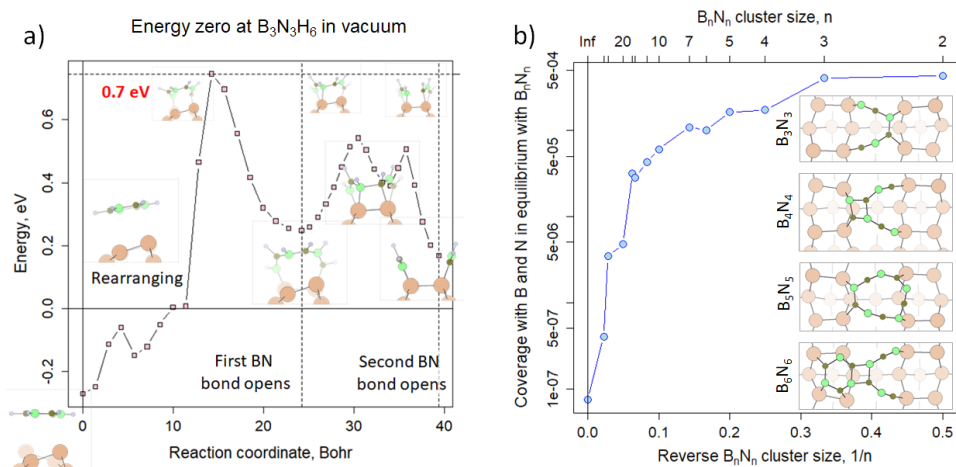


Figure 2. (a) Dissociative adsorption of $B_3N_3H_6$ on Ge(001): the path by direct BN ring splitting. The molecule in the leftmost insets is physisorbed, the rightmost insets show $B_3N_3H_6$ split into BN_2H_3 and B_2NH_3 . B is brown, N is green, H is blue, Ge is sepia. (b) Ge(001) coverage with B and N atoms in equilibrium (900°C) with B_nN_n .

3.1 Nucleation and Growth of hBN from $B_3N_3H_6$ on Ge(001)

$B_3N_3H_6$ physisorbs on Ge(001) with no barrier, gaining 0.3 eV (Fig. 2a, leftmost insets). At the processing conditions, the barriers for subsequent chemisorption are surmounted readily. For instance, when a H atom jumps from $B_3N_3H_6$ onto Ge, a pair of chemisorbed H and $B_3N_3H_5$ appears. The barrier depends on whether the dehydrogenated atom is B (0.4 eV, GeB bond formed) or N (0.7 eV, GeN bond formed). Alternatively, the physisorbed molecule splits into BN_2H_3 and B_2NH_3 (the barrier is 0.7 eV, Fig. 2a) and these fragments separate with a barrier of 1.8 eV (*i. e.*, within the range typical for objects mobile on Ge).

The adsorbed fragments are mobile and unstable: they collect H and desorb, or lose H and become more strongly bonded, or polymerise. $B_3N_3H_5$ can split by an H-assisted reaction similar to that shown in Fig. 2a. It is unclear if further opening of BN bonds is viable (although a BN dimer splits into B and N atoms), but what is crucial for the monolayer grow is that precursors with split BN rings are available. Namely, closed rings can produce only stoichiometric hBN with armchair edges, while with half-ring precursors any shape and any chemically realistic deviation from stoichiometry can be achieved.

The flake edges are strongly bonded to the substrate. For example, nearly all B and N atoms of a flake with its armchair edge perpendicular to dimer rows on flat Ge(001) make bonds with Ge atoms. At 900°C and H_2 partial pressures around 10^{-3} mbar (the processing conditions), H occupies about 0.1% of all edge atoms. Solely at H_2 pressures in the atmospheric regime (*e. g.*, at 100 mbar) this occupation may reach a few per cent.

The hBN flakes grow in a manner similar to that of graphene (Sec. 2): a cluster nucleated by chance collects material from its surrounding. Fig. 2b illustrates this on the example of the growth from atomic B and N. As the flake grows, the concentration of B and N in the surrounding decreases, reflecting the increasing stability of the flake. B_nN_n clusters with n equal to or barely exceeding 6 do not form sixfold rings (Fig. 2, insets).

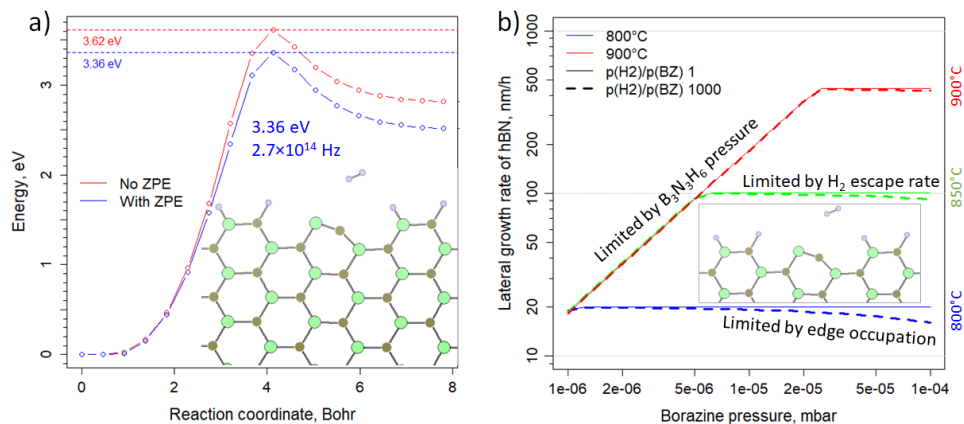


Figure 3. (a) Spontaneous H_2 emission from the hBN armchair edge, with and without Zero Point Energy (ZPE) correction. In the inset, N is green, B is brown, and H is blue. (b) Step flow velocity during growth of multilayer hBN. The hydrogenated sites are passive, only the H-free sites can adsorb $\text{B}_3\text{N}_3\text{H}_6$ from the gas phase. The attempt rate for spontaneous H_2 emission from armchair hBN edges was estimated from the transition state theory. The steric factor for $\text{B}_3\text{N}_3\text{H}_6$ attachment to an H-free site on the step edge is assumed to be 1.

This is an edge effect: such short or open rings occur on edges of even large flakes.

3.2 Growth of Multilayer hBN Films

Instead of stopping when the catalyst is fully covered by a single layer of the passive film, the hBN growth continues indefinitely. But no multilayer graphene would grow at comparable conditions from C_6H_6 (equivalent of $\text{B}_3\text{N}_3\text{H}_6$), and not even from more reactive CH_4 , unless the precursors have been activated. Activation is thus expected also during hBN growth. We found that it must occur on hBN edges (Fig. 3a). In contrast to what happens on graphene, H_2 emission can keep the hBN growth front free of hydrogen even below 850°C (Fig. 3b). The sticking coefficient of $\text{B}_3\text{N}_3\text{H}_6$ to a hydrogen-free BN dimer is close to 1 because the energy barrier for this attachment is zero within the accuracy of the calculations and the molecule is pre-oriented by preliminary physisorption on the hBN surface. The armchair edge is free of hydrogen when the partial pressure of H_2 is 10^{-6} mbar; even when it is increased to 10^{-2} mbar, only a few per cent of the edge sites are passivated. At the $\text{B}_3\text{N}_3\text{H}_6$ partial pressure of 10^{-6} mbar the time to reach this equilibrium is only marginally longer than the average time that elapses between two subsequent collisions of $\text{B}_3\text{N}_3\text{H}_6$ with the edge. The attempt rate for H_2 escape from the dimer was estimated as $3 \cdot 10^{14}$ Hz. The growth rate obtained from the computed step flow velocity (Fig. 3b) and from the step-step distance estimated from TEM images agrees within the numerical and experimental uncertainties with the observed growth rates.

We have also tested the hypothesis that another process is responsible for the activation. We considered the possibility of H out-diffusion along screw dislocations in hBN from the growth front onto Ge, of catalytic activation of $\text{B}_3\text{N}_3\text{H}_6$ to $\text{B}_3\text{N}_3\text{H}_4$ or of H_2 to atomic H on hot elements in the chamber, and of catalytic activation of $\text{B}_3\text{N}_3\text{H}_6$ on orientational grain boundaries in hBN. The mechanism on the second place in the plausibility ranking is the

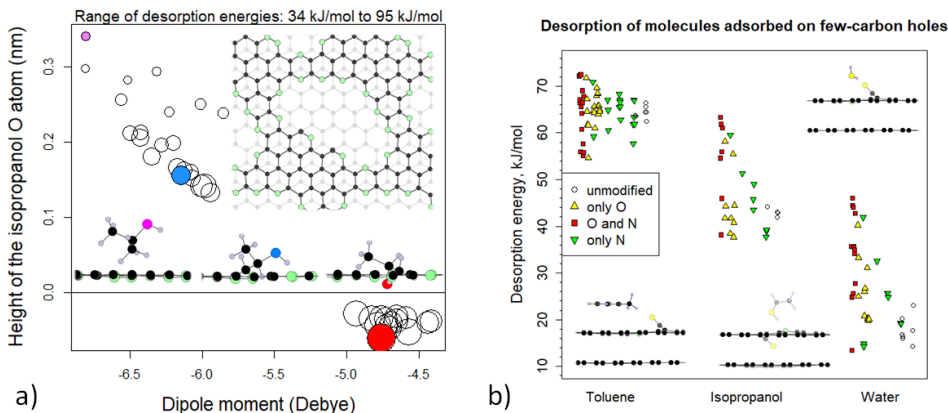


Figure 4. (a) Correlation between dipole moment, oxygen penetration depth, and desorption energy (circle diameter) for a hole in the top layer of bilayer graphene (inset, top view). The hole edge is saturated by pyridine N. (b) Overview of desorption energies computed for toluene, isopropanol, and water adsorbed on various few-atom holes with various N and O functional groups. The insets illustrate the strongest adsorption cases (side view).

activation on hot elements, but it appears to be incompatible with the possibility to grow hBN at temperatures and pressures well below the limits estimated from the calculations. Therefore, spontaneous H_2 emission (Fig. 3) comes out as the only known realistic answer.

4 Examples of Work in Progress

4.1 Catalytic Activity of 2D Films

Activated carbons have enormous application potential as catalysts³⁰, *e. g.* in the oxidative dehydrogenation of hydrocarbons³¹ or in the oxidation of SO_2 to SO_3 ³². Defects and anchors of functional groups influence the surface interactions with the molecules from the liquid or gas phase and their activation towards catalytic transformations³³.

Catalytic activity of a surface begins with adsorption of the participating species. We currently investigate the influence of N and O functional groups on adsorption of test molecules on openings in bilayer graphene (Fig. 4). The model substrate is periodic to assure that its density of states is metallic, as in our experiments²⁵, in which structurally comparable samples of porous activated carbon are prepared by pyrolysis of sucrose ($C_{12}O_{11}H_{22}$), pure or with urea ($CO(NH_2)_2$) admixtures. The calculations show that the desorption energy of isopropanol (C_3H_7OH , a polar test molecule that is able to form hydrogen bonds through its OH group) correlates positively with the reduction of the dipole moment in the adsorbate-substrate system; this corresponds to the molecule being partially drawn into the opening (Fig. 4a). Nitrogen doping of an O-containing substrate has the tendency to increase the desorption energies of isopropanol and water even when the openings are only of the size of a few C atoms, but the effect on toluene ($C_6H_5CH_3$, non-polar test molecule that forms no hydrogen bonds) is practically non-existent (Fig. 4b).

Experimental verification of the computed desorption energies by temperature programmed desorption (TPD) measurements turned out to be difficult. The activation en-

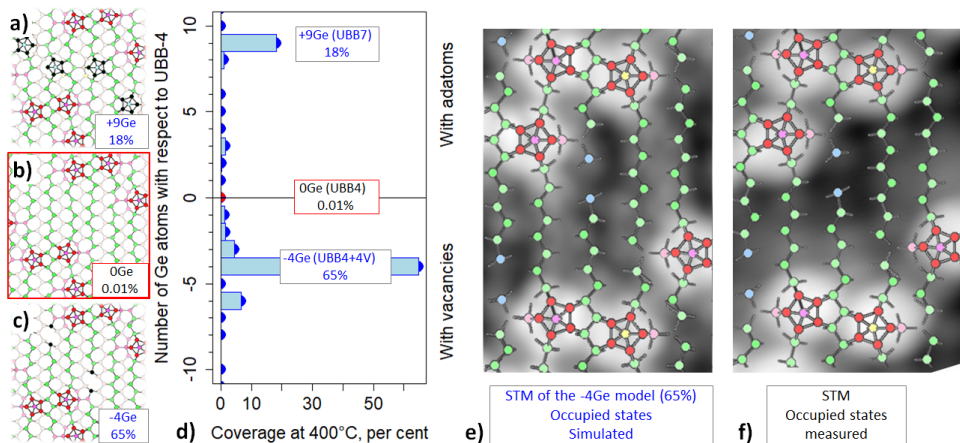


Figure 5. Ge(110) reconstructions. (a-c) Representative 8×10 reconstruction models. Pentamers are red, ordinary (110) zig-zag atoms are green. (a) The densified UBB7 model (+9Ge, 18% at 400°C), the additional pentamers are black. (b) The original UBB4 model²⁷ (0Ge, abundance 0.01%). (c) The UBB4+4V model (-4Ge, 65%) is on the bottom, the vacancy neighbours are black. (d) Approximate abundance of structures with various net balance of Ge atoms. (e-f) STM images of occupied states. (e) simulated for UBB4+4V, (f) measured.

ergies extracted from the heating rate dependence of the TPD spectra were unphysically low, which indicates that the spectra were dominated by desorption from long nano-pores, where re-adsorption and bottlenecks in the gas flow play the dominant role. Experiments on samples prepared by a modified procedure are in progress.

4.2 Ge(110) Surface Reconstruction

Knowing the atomic structure of a surface is prerequisite for reliable simulation and in-depth explanation of chemical and atomic-scale surface processes (Sec. 2). Clean Ge(110) is covered by objects visible in STM images as pentamers of atomic-sized spots. After long anneals these pentamers tend to arrange in rows separated from one another by strips of apparently flat surface (Fig. 5f). The atomic origin of the pentamers has been the subject of a long debate. We reconciled two structural models recently proposed for these pentamers: the adatom-based Universal Building Block model (UBB)²⁷ (Fig. 5b, 0Ge or UBB4) and the vacancy-based Tetramer Heptagonal- and Tetragonal Ring model (THTR)²⁶. The search for a new model was motivated by our discovery that in contrast to the expectations from experiments, the UBB4 Ge(110) 8×10 surface has a tendency to acquire additional UBB pentamers (Fig. 5a, +9Ge or UBB7). This behaviour is suppressed and the surface energy is reduced when the UBB4 structure is augmented by two vacancy pairs (Fig. 5c, -4Ge or UBB4+4V), each rebonded as in THTR. The STM images simulated for this model are compatible with experiment (Fig. 5e-f).

5 Approach

Pseudopotential plane-wave DFT calculations were done with Quantum Espresso³⁴ using the PBE functional³⁵ and in special cases by the hybrid B3LYP functional^{36,37}. Van der

Waals forces were treated as non-local DFT (rVV10)³⁸. Reaction paths were determined with the nudged elastic band - climbing image (NEB-CI) algorithm³⁹. The accuracy of pseudopotential calculations for isolated molecules was verified by all-electron calculations with NWChem⁴⁰, using the double-hybrid B2PLYP⁴¹ functional. Vibrational spectra were computed within the density functional perturbation theory (DFPT)⁴².

6 Concluding Remarks

Insight into problems pertinent to materials development for environmentally friendly technologies was obtained from DFT simulations coupled to experiment. The difference in the surface evolution of Ge(001) and Ge(110) in response to graphene growth by CVD was explained (Sec. 2) and, as a fringe benefit, a structural model reconciling two dissimilar concepts of Ge(110) reconstructions was formulated (Sec. 4.2). The growth mechanism of seeding (on Ge) and growth of multilayer hBN films was proposed and positively verified against the measured growth rates (Sec. 3). The role of N/O co-doping of activated carbon in adsorption of polar and non-polar molecules was addressed (Sec. 4.1).

Acknowledgements

The calculations were performed with a grant of computer time provided by the John von Neumann Institute for Computing on the JUWELS cluster at the Jülich Supercomputing Centre (JSC) in the compute projects IHPms21 and IHPms24. J. D., F. A., M. F., and M. L. gratefully acknowledge funding from the EU FLAG-ERA project 2DHetero²⁴. Also the financial support by the German Research Foundation (DFG; grant Nr. KL 1202/17-1)²⁵ of the experimental work on the activated carbon is highly appreciated. We thank Andreas Becker for STM measurements.

References

1. C. L. Lai and S. H. Lin, *Treatment of chemical mechanical polishing wastewater by electrocoagulation: system performances and sludge settling characteristic*, *Chemosphere*, **54**, 235, 2004.
2. E. A. Noman et al., *An insight into microelectronics industry wastewater treatment, current challenges, and future perspectives: a critical review*, *Applied Water Science*, **14**, 64, 2024.
3. Y. Liu, H. Wang, Y. Cui, and N. Chen, *Removal of Copper Ions from Wastewater: A Review*, *International Journal of Environmental Research and Public Health*, **20**, no. 5, 2023.
4. X. Li, H. Jin, Y. Chan, H. Guo, and W. Ma, *Environmental impacts of graphene at industrial production scale and its application in electric heating technology*, *Resources, Conservation and Recycling*, **199**, 107250, 2023.
5. Y. Chen, X.-L. Gong, and J.-G. Gai, *Progress and Challenges in Transfer of Large-Area Graphene Films*, *Advanced Science*, **3**, 1500343, 2017.

6. R. Arvidsson, D. Kushnir, S. Molander, and B. A. Sandén, *Energy and resource use assessment of graphene as a substitute for indium tin oxide in transparent electrodes*, *Journal of Cleaner Production*, **132**, 289, 2016.
7. A. Ambrosi and M. Pumera, *The CVD graphene transfer procedure introduces metallic impurities which alter the graphene electrochemical properties*, *Nanoscale*, **6**, 72, 2014.
8. G. Lupina, J. Kitzmann, I. Costina, M. Lukosius, C. Wenger, A. Wolff, S. Vaziri, M. Östling, I. Pasternak, A. Krajewska, W. Strupinski, S. Kataria, A. Gahoi, M. C. Lemme, G. Ruhl, G. Zoth, O. Luxenhofer, and W. Mehr, *Residual metallic contamination of transferred chemical vapor deposited graphene*, *ACS nano*, **9**, 4776, 2015.
9. G. Lippert, J. Dabrowski, T. Schroeder, Y. Yamamoto, F. Herziger, J. Maultzsch, J. Baringhaus, C. Tegenkamp, M. C. Asensio, J. Avila, and G. Lupina, *Graphene on Ge(001) from atomic source*, *Carbon*, **75**, 104, 2014.
10. J. Dabrowski, G. Lippert, J. Avila, J. Baringhaus, I. Colambo, Yu. S. Dedkov, F. Herziger, G. Lupina, J. Maultzsch, T. Schaffus, T. Schroeder, M. Sowinska, C. Tegenkamp, D. Vignaud, and M.-C. Asensio, *Understanding the growth mechanism of graphene on Ge/Si(001) surfaces*, *Sci. Rep.*, **6**, 31639, 2016.
11. M. Lukosius et al., *Metal-Free CVD Graphene Synthesis on 200 mm Ge/Si(001) Substrates*, *ACS Appl. Mater. Interfaces*, **8**, 33786, 2016.
12. F. Akhtar, J. Dabrowski, R. Lukose, C. Wenger, and M. Lukosius, *Chemical Vapor Deposition Growth of Graphene on 200 mm Ge(110)/Si Wafers and Ab Initio Analysis of Differences in Growth Mechanisms on Ge(110) and Ge(001)*, *ACS Appl. Mater. Interfaces*, **15**, 36966, 2023.
13. F. Akhtar, *Graphene synthesis under Si-CMOS compatible conditions*, PhD thesis, BTU Cottbus, April 2022.
14. A. Becker, Ch. Wenger, and J. Dabrowski, *Influence of temperature on growth of graphene on germanium*, *J. Appl. Phys.*, **128**, 2020.
15. J. Dabrowski and V. Zavodinsky, *Ab initio study of Pr oxides for CMOS technology*, *NIC Series*, **20**, 171, 2004.
16. J. Dabrowski, A. Fleszar, G. Lippert, and G. Lupina, *Ab initio modelling of growth of graphene for Si-compatible microelectronics*, *NIC Series*, **47**, 207, 2014.
17. J. Dabrowski, G. Lippert, and G. Lupina, *Nucleation of graphene on the Ge(001) $p2 \times 2$ surface*, *NIC Symposium*, **8**, MAT 6, 2016.
18. J. Dabrowski, G. Kissinger, G. Lippert, G. Lupina, M. Lukosius, P. Sana, and T. Schroeder, *Modelling of materials for silicon-compatible microelectronics*, *NIC Series*, **49**, 239, 2018.
19. J. Dabrowski, F. Reichmann, M. Franck, and M. Lukosius, *Ab initio simulations for microelectronics: $ZnGa_2O_4$ and hexagonal BN*, *NIC Series*, **51**, 245, 2022.
20. M. Franck, J. Dabrowski, M. A. Schubert, C. Wenger, and M. Lukosius, *Towards the Growth of Hexagonal Boron Nitride on Ge(001)/Si*, *Nanomaterials*, **12**, 3260, 2022.
21. M. Franck, J. Dabrowski, M. A. Schubert, D. Vignaud, M. Achehboune, J.-F. Colomer, L. Henrard, C. Wenger, and M. Lukosius, *Investigating impacts of local pressure and temperature on CVD growth of hexagonal boron nitride on Ge(001)/Si*, *Advanced Materials Interfaces*, **12**, 2400467, 2024.

22. W. Batista-Pessoa, M. Franck, N. Nuns, J. Dabrowski, M. Achehboune, J.-F. Colomer, L. Henrard, M. Lukosius, X. Wallart, and D. Vignaud, *Optimized two-step growth of large surface two-dimensional boron nitride on Ge(001) films by molecular beam epitaxy*, submitted to Applied Surface Science, 2024.
23. M. Achehboune, K. Zhou, J. Dabrowski, D. Vignaud, M. Franck, M. Lukosius, J.-F. Colomer, and L. Henrard, *Atomistic insights into the nucleation and growth of hexagonal boron nitride and graphene heterostructures*, Phys. Chem. Chem. Phys., **26**, 28198, 2024.
24. “2DHetero: hBN/graphene 2D Heterostructures: from scalable growth to integration”, EU FLAG-ERA project.
25. O. Klepel, “Interplay of nitrogen- and oxygen functionalities of carbon based catalysis in redox reactions”, DFG, KL1202/17-1, since 2019.
26. T. Yamasaki, K. Kato, T. Uda, and T. Yamamoto, *First-principles theory of Si(110)-(16 × 2) surface reconstruction for unveiling origin of pentagonal scanning tunneling microscopy images*, Applied Physics Express, **9**, 035501, 2016.
27. R. A. Zhachuk and A. A. Shklyae, *Universal building block for (110)-family silicon and germanium surfaces*, Applied Surface Science, **494**, 46, 2019.
28. D. Akinwande, C. Huyghebaert, C.-H. Wang, M. I. Serena, S. Goossens, L.-J. Li, H-S. P. Wong, and F. H. L. Koppens, *Graphene and two-dimensional materials for silicon technology*, Nature, **573**, 507, 2019.
29. J. Dabrowski, G. Lippert, and G. Lupina, *Initial state of graphene growth on Ge(001) surfaces*, ECS Transactions, **69**, 345, 2015.
30. X. Liu, A. Cheruvathur, and R. Sharpe, *Carbon-based metal-free catalysis for dehydrogenation of hydrocarbons*, in: Metal-free Functionalized Carbons in Catalysis: Synthesis, Characteris, and Applications, The Royal Soc. Chem., 196, 2018.
31. I. Szewczyk et al., *Electrochemical Denitrification and Oxidative Dehydrogenation of Ethylbenzene over N-doped Mesoporous Carbon: Atomic Level Understanding of Catalytic Activity by 15N NMR Spectroscopy*, Chem. Mater., **32**, 7263, 2020.
32. E. Raymundo-Piñero, D. Cazorla-Amorós, C. Salinas-Martinez de Lecea, and A. Linares-Solano, *Factors controlling the SO₂ removal by porous carbons: relevance of the SO₂ oxidation step*, Carbon, **38**, 335, 2000.
33. E. Vottero et al., *Assessing the functional groups in activated carbons through a multi-technique ap-proac*, Catal. Sci. Technol., **12**, 1271, 2022.
34. P. Giannozzi et al., *QUANTUM ESPRESSO: a modular and open-source software project for quantum simulations of materials*, J. Phys. Cond. Mat., **21**, 395502, 2009, see also: What Can Quantum Espresso Do? <http://www.quantum-espresso.org/whatcandedo.php>.
35. J. P. Perdew, K. Burke, and M. Ernzerhof, *Generalized gradient approximation made simple*, Phys. Rev. Lett., **77**, 3865, 1996.
36. A. D. Becke, *Density-functional thermochemistry. III. The role of exact exchange*, J. Chem. Phys., **98**, 5648, 1993.
37. P. J. Stephens, F. J. Devlin, C. F. Chabalowski, and M. J. Frisch, *Ab Initio Calculation of Vibrational Absorption and Circular Dichroism Spectra Using Density Functional Force Fields*, J. Phys. Chem., **98**, 11623, 1994, and references therein.
38. R. Sabatini, T. Gorni, and S. de Gironcoli, *Nonlocal van der Waals density functional made simple and efficient*, Phys. Rev. B, **87**, 041108(R), 2013.

39. G. Henkelman, B. P. Uberuaga, and H. Jónsson, *A climbing image nudged elastic band method for finding saddle points and minimum energy paths*, J. Chem. Phys., **113**, 9901, 2000.
40. E. Apra et al., *NWChem: Past, present, and future*, J. Chem. Phys., **152**, 184102, 2020.
41. S. Grimme, *Semiempirical hybrid density functional with perturbative second-order correlation*, J. Chem. Phys., **124**, 34108, 2006.
42. S. Baroni et al., *Phonons and related properties of extended systems from density-functional perturbation theory*, Rev. Mod. Phys., **73**, 515, 2001.